Analysis of Ar $3p^6$ and Kr $4p^6$ photoionization from photoelectron-spin-polarization data

F. Schäfers, G. Schönhense, and U. Heinzmann

Fritz-Haber-Institut der Max-Planck-Gesellschaft, Faradayweg 4-6, D-1000 Berlin 33, West Germany

Experimental data of the cross section and of the asymmetry parameter β in combination with photoelectron-spin-polarization results of Ar $3p^6$ and Kr $4p^6$ subshell photoionization were used to determine the bound-free matrix elements and phase-shift differences of the continuum wave functions in a photon-energy region from threshold to 41 eV. The paper includes a discussion of the first autoionization region between the $^2P_{3/2}$ and $^2P_{1/2}$ thresholds in the framework of the angular-momentum-transfer formalism. The experimental results are compared with semiempirical and *ab initio* calculations with the use of line positions and oscillator strengths in the discrete part extrapolated to the continuum in application of the multichannel quantum-defect theory.

I. INTRODUCTION

The photoabsorption and photoionization process of the rare gases has been the subject of theoretical and experimental work for more than half a century. Since Beutler published his well-known resonance absorption profiles nearly all theoretical photoionization models first have been applied to and tested on the rare gases, particularly the p subshell, as this is the simplest case: the photoionization of a closed outermost subshell. Experimental material first consisted primarily of photoabsorption and photoionization cross sections, but during the last decade studies of the photoelectron angular distributions became dominant and in recent years the photoelectron spin polarization was of interest. It turned out that only the most sophisticated models could describe all the experimental data satisfactorily. Relativistic effects (i.e., spin-orbit interaction) both in the ground and in the continuum states had to be taken into account as well as many-electron correlations within the subshell considered and between different subshells.

The photoionization of a p subshell is theoretically described in the relativistic model by $3+2$ bound-free dipole matrix elements (transitions from the $np_{3/2}$ ground state into the energy-degenerate continua $\epsilon s_{1/2}$, $\epsilon d_{3/2}$, and $\epsilon d_{5/2}$ and from the $np_{1/2}$ state into the $\epsilon s_{1/2}$ and $\epsilon d_{3/2}$ continua, respectively) and by the $2+1$ relative phases of the electron continuum wave functions. (For a detailed theoretical treatment, see, e.g., Ref. 1.) All experimental quantities measured so far are, respectively, functions of these five and three parameters.

Therefore, from the experimental point of view a set of five independent measurements yields a complete parameter set for the description of the photoionization of a $p_{3/2}$ subshell, while only three measurements are needed in the case of the $p_{1/2}$ subshell. The following parameter set was introduced by Cherepkov[2] and Lee[3]:

(1) subshell cross section σ;

(2) asymmetry parameter β of the differential cross section;

(3) spin parameter ξ (photoelectron polarization normal to the reaction plane);

(4) angle-integrated spin-polarization transfer A from

circularly polarized radiation to photoelectrons;

(5) asymmetry parameter α of the angle-resolved spin-polarization transfer.

For the measurement of parameters (1)—(3) unpolarized or linearly polarized light can be used, while parameters (4) and (5) must be measured with circularly polarized light. It is worth noting that the five dynamical parameters mentioned are functions of the light energy as well as of the photoelectron kinetic energy.

Spin-polarization measurements are connected with an intensity loss of 10^3 due to the use of Mott scattering as an analyzing device. Therefore, up until now, only the highest-intensity rare-gas lamps could be used for measurements of ξ where the photoelectron emission has to be resolved simultaneously with respect to energy, angle, and spin. Using circularly polarized light, a spin polarization remains, however, even if one extracts all electrons regardless of their direction of emission. The parameter A is defined as the ratio of the electron's spin polarization to the circular polarization of the ionizing light. Elliptically polarized vacuum ultraviolet radiation with a high degree of circular polarization has become feasible by use of the off-axis radiation of a synchrotron or a storage ring. As the intensity of the circularly polarized synchrotron radiation is three orders of magnitude lower than the unpolarized light of the rare-gas lamps, up until now no measurements of the spin asymmetry parameter α could be performed. Such measurements are, however, in progress at the new German dedicated storage ring BESSY.

While the cross section is determined only by squares of the dipole matrix elements, the dynamical parameters (2)—(5) are sensitive to the phases of the continuum functions. It is the purpose of this paper to present an analysis of Ar $3p^6$ and Kr $4p^6$ photoionization in the photon-energy range from threshold to 41 eV taking all experimental results as the basis for this analysis i.e., to present the matrix elements and phase-shift differences of the continuum functions determined individually with the use of experimental quantities only. It is straightforward that these quantities are very sensitive in testing atomic theories, more so than the dynamical parameters which are functions of more than one matrix element and phase. The paper includes a discussion of the Beutler-Fano au-

toionization resonances, based on measurements of the spin polarization, in the framework of the angular-momentum-transfer theory. These data will be compared with data determined semiempirically and *ab initio* from line positions and oscillator strengths in the discrete part of the spectrum extrapolated into the continuum along the lines given by the multichannel quantum-defect theory (MQDT).

The rare gases Ar and Kr have been chosen because a lot of experimental and theoretical work exists which such an analysis can be based upon; in combination with a corresponding analysis of Xe by Heinzmann[4] it allows a detailed comparison of the behavior of the parameters and of the relative importance of spin-orbit effects and correlations going from the lighter to the heavier atoms.

The main part of the experimental studies in the autoionization region between the fine-structure-split $^2P_{3/2}$ and $^2P_{1/2}$ thresholds concentrated on the cross section [Ar (Refs. 5—11) and Kr (Refs. 9—15)] which exhibits pronounced resonance structure due to two series of Beutler-Fano resonances converging to the $^2P_{1/2}$ threshold. Measurements of the β parameter in this region were reported only for Xe by Samson and Gardner.[16] Studies of spin polarization with circularly polarized synchrotron radiation were performed by Heinzmann and Schäfers[17] for Ar and Kr and by Heinzmann et al.[18] for Xe. Theoretical treatments of the autoionization resonances have widely been based on MQDT. The first prediction of the behavior of spin-polarization parameters was made by Lee.[3] Empirical MQDT parameters obtained from electron energy-loss measurements were used by Geiger for autoionization studies of Kr and Xe,[19,20] while Dill[21] computed the β parameter for Xe. The most recent analysis was performed by Johnson et al.[22] who employed *ab initio* parameters determined in the relativistic random-phase approximation (RRPA).

Photoionization in the smooth spectral range above the $^2P_{1/2}$ threshold was studied by a number of workers. The cross-section measurements[6,9,23—26] have been summarized by Marr and West.[27] The branching ratio was measured by Comes and Sälzer[28] and Samson et al.[29,30] Extended investigations of the β parameter are available. Most experiments were done with line sources,[31—43] some with synchrotron radiation.[44—51] The measurements of β and the branching ratio have recently been extended to the inner-shell autoionization region with the use of synchrotron radiation.[52] The spin-polarization parameter ξ was measured by Heinzmann et al.[53] with the use of unpolarized light, while circularly polarized synchrotron radiation was used for the determination of the spin-polarization transfer A.[17,18]

In contrast to the theoretical treatment of the photoionization cross section of the rare gases, only very few *ab initio* calculations of photoelectron polarization exist. The experimental results may be compared with the nonrelativistic random-phase approximation with exchange (RPAE) calculations of Cherepkov,[2,54—56] with RRPA computations of Johnson and Cheng[57] and Huang et al.[58—60] and with considerations by Klar[61] in the formalism of angular-momentum transfer.

After a brief description of the experimental designs used for the spin-polarization measurements (Sec. II), the "experimental" matrix elements and phase-shift differ-

ences will be presented in Sec. III. together with a survey of the MQDT guiding this analysis. As an application in Sec. IV the results of Sec. III are compared with *ab initio* calculations. Section V presents a comparison of the spin-polarization measurements in the autoionization region with different calculations and a further analysis of the resonance structure by means of the angular-momentum-transfer formalism.

II. EXPERIMENTAL ARRANGEMENT

The experimental arrangement for the investigation of the photoelectron spin polarization normal to the reaction plane, described by the parameter ξ, was explained previously.[62] Briefly, unpolarized light from rare-gas discharge lamps intersects an atomic beam in a region free of electric and magnetic fields. The photoelectrons produced in the interaction volume and ejected into a certain direction of emission pass through an electron spectrometer (cylindrical mirror analyzer) and are accelerated to 120 keV for spin-polarization analysis by means of a Mott detector. The angular dependence of this polarization component is given by[2,3]

$$P(\theta) = \frac{2\xi \sin\theta \cos\theta}{1 - (\beta/2)P_2(\cos\theta)} \ .$$

The parameter ξ can be directly obtained from the measured polarization P when the experiment is carried out under the "magic" angle $\theta_m = 54°44'$ (the angle between photon and electron momentum): $\xi = 1.061P(\theta_m)$.

For the studies of the spin-polarization transfer A the off-axis radiation of the Bonn synchrotron was used which was found to be largely circularly polarized.[63] Briefly, the polarized vuv radiation was imaged onto the exit slit of a 10-m normal-incidence monochromator (bandwidth 0.08 nm). All photoelectrons ejected from the atomic beam were extracted by an electric field and accelerated to 120 keV for subsequent polarization detection. Due to the extraction procedure no energy analysis of the extracted electrons could be performed. Therefore, this arrangement is best suited for the investigation of the outermost shell, where no two sorts of electrons with different kinetic energies have to be separated, i.e., from outer s subshells[64] or in the autoionization region between the two fine-structure-split thresholds of the rare gases where, furthermore, the advantage of a continuous light source to step through the resonances comes largely into effect.

III. EVALUATION OF MATRIX ELEMENTS AND PHASE-SHIFT DIFFERENCES OF THE CONTINUUM WAVE FUNCTIONS FOR Ar AND Kr FROM THE EXPERIMENTAL RESULTS

A. Theoretical background

During the last decade Fano, Lu, and Lee[3,65—71] developed the MQDT from the basic ideas of Sommerfeld[72] and Seaton.[73,74] In these works a formalism was set up which allowed one to describe positions and intensity distributions of spectral lines that belong to strongly interacting, i.e., disturbed Rydberg series. The validity of the theory extends, however, beyond the discrete spectral range into the adjacent autoionization range and the ioni-

zation continuum where, for instance, the interaction of discrete excited states with continuum states is explained resulting in autoionization resonances with the typical Beutler-Fano profiles (Sec. V).

In the MQDT the concept of channels is introduced with intent to represent the position and intensity of all spectral lines and autoionization resonances in a small set of parameters. The theory connects the close-coupling eigenchannels α (classified approximately by LS quantum numbers) with the loose-coupling dissociation channels i of the ion plus electron system (classified exactly in the jj-coupling scheme). The system transformation is represented by an orthonormal matrix $U_{i\alpha}$, in which configuration interaction and channel mixing are taken into account. For the rare gases $U_{i\alpha}$ has been calculated ab initio[22,68] or has been determined semiempirically from spectroscopic data.[19,20,69]

Due to the selection rules the following channels are open for dipole transitions from the ground state $np^6\,{}^1S_0$ of the rare gases: close-coupling states (eigenchannels)

$$p^5d\,{}^3P_1, \quad p^5d\,{}^3D_1, \quad p^5d\,{}^1P_1,$$

$$p^5s\,{}^3P_1, \quad p^5s\,{}^1P_1$$

for $\alpha = 1-5$, respectively, and loose-coupling states (dissociation channels)

$$({}^2P_{3/2}d_{5/2})_1, \quad ({}^2P_{3/2}d_{3/2})_1, \quad ({}^2P_{3/2}s_{1/2})_1$$

$$({}^2P_{1/2}d_{3/2})_1, \quad ({}^2P_{1/2}s_{1/2})_1$$

for $i = 1-5$, respectively.

The system transformation is performed by the following equation:

$$D_i e^{i\pi\mu_i} = \sum_{\alpha=1}^{5} U_{i\alpha} D_\alpha e^{i\pi\mu_\alpha} . \tag{1}$$

The weakly energy-dependent eigen-quantum-defects μ_α and the transition amplitudes D_α determine the energetic position and the intensity (oscillator strength) of the spectral lines,[65] respectively. These data of the discrete spectral range may therefore be transformed into the "modified" quantities D_i and μ_i by use of the matrix $U_{i\alpha}$. In the

ionization continuum the D_i represent the reduced dipole matrix elements of photoionization, whereas the modified quantum defects μ_i are the non-Coulombic part of the phase shifts δ_i of the continuum wave functions in units of π:

$$\delta_i = \sigma_l + \pi\mu_i - \pi l/2 . \tag{2}$$

σ_l is the Coulomb or long-range phase shift of the partial wave l that occurs because the photoelectron leaves in the Coulomb potential of the singly positive charged ion. $\pi\mu_i$ denotes the short-range phase shift of the continuum wave function and is due to deviations of the true potential from the pure Coulomb potential close to the atom. $\pi l/2$ is a normalization term of the phases which determines the right sign of the matrix elements. The Coulomb phases can be calculated analytically[75]:

$$\sigma_l = \arg\Gamma(l+1-i\epsilon^{-1/2}) , \tag{3}$$

where ϵ is the electron's kinetic energy in rydberg units.

B. Evaluation procedure

The matrix elements D_i and the differences of the modified eigen-quantum-defects $\mu_i - \mu_j$ have been determined by use of experimental results obtained in the continuous spectral range and are compared with spectropscopic data below the ionization threshold according to Eq. (1). The evaluation procedure for D_i and $\mu_i - \mu_j$ described by Heinzmann[4] is sketched out only briefly in the following.

First, the experimental parameters are expressed as functions of the matrix elements D_i and the phase-shift differences δ_i. σ, the cross section for the photoionization of the np^6 valence shell; ρ, branching ratio $\sigma_{3/2}/\sigma_{1/2}$ of the spin-orbit components; $\beta_{3/2}$ and $\beta_{1/2}$, asymmetry parameter of the differential cross section; $\xi_{3/2}$ and $\xi_{1/2}$, spin-polarization parameter; and $A_{3/2}$ and $A_{1/2}$, angle-integrated spin-polarization transfer, are expressed as follows:

$$\sigma = 4\pi^2 \alpha a_0^2 \omega \sum_{i=1}^{5} D_i^2 \tag{4}$$

with α the fine-structure constant, a_0 the Bohr radius, and ω the photon energy in a.u.,

$$\rho = \frac{D_1^2 + D_2^2 + D_3^2}{D_4^2 + D_5^2} = \frac{\sigma_{3/2}}{\sigma_{1/2}} , \tag{5}$$

$$\beta_{3/2} = \frac{4D_1^2 - 4D_2^2 + 6D_1D_2\cos(\delta_1 - \delta_2) - 2\sqrt{5}D_2D_3\cos(\delta_2 - \delta_3) - 6\sqrt{5}D_3D_1\cos(\delta_3 - \delta_1)}{5(D_1^2 + D_2^2 + D_3^2)} , \tag{6}$$

$$\beta_{1/2} = \frac{D_4^2 + 2\sqrt{2}D_5D_4\cos(\delta_5 - \delta_4)}{D_4^2 + D_5^2} , \tag{7}$$

$$\xi_{3/2} = \frac{15D_1D_2\sin(\delta_1 - \delta_2) + 3\sqrt{5}D_2D_3\sin(\delta_2 - \delta_3) + 6\sqrt{5}D_3D_1\sin(\delta_3 - \delta_1)}{20(D_1^2 + D_2^2 + D_3^2)} , \tag{8}$$

$$\xi_{1/2} = \frac{3\sqrt{2}D_5D_4\sin(\delta_5 - \delta_4)}{4(D_4^2 + D_5^2)} , \tag{9}$$

$$A_{3/2} = \frac{7D_1^2 - 2D_2^2 - 5D_3^2 - 12D_1D_2\cos(\delta_1 - \delta_2)}{10(D_1^2 + D_2^2 + D_3^2)} , \tag{10}$$

$$A_{1/2} = \frac{D_5^2 - 0.5D_4^2}{D_4^2 + D_5^2} . \tag{11}$$

The quantities correspond to the following final ionic states. To $^2P_{3/2}$,

$$D_1, \quad D_2, \quad D_3, \quad \delta_1-\delta_2, \quad \delta_3-\delta_1,$$

$$\delta_2-\delta_3 = -(\delta_1-\delta_2)-(\delta_3-\delta_1) ,$$

and to $^2P_{1/2}$,

$$D_4, \quad D_5, \quad \delta_5-\delta_4 .$$

Only σ depends on the absolute magnitude of the matrix elements. All other parameters are determined by ratios of matrix elements only. $A_{1/2}$ does not depend on the phase difference. $A_{3/2}$ depends only on the phase difference between the two d partial waves $\delta_1-\delta_2$, of which the difference of the Coulomb phases is zero according to Eq. (2). Only ξ is determined by the sine, i.e., an odd trigonometric function of the phase difference, because the terms in the numerator of ξ are imaginary parts of products of complex matrix elements.[1]

It is worth noting that the five matrix elements and three phase-shift differences totaling eight quantities represent a complete parameter set only in the loose-coupling scheme and for the case of p^6-subshell ionization. In general, the transformation matrix $U_{i\alpha}$ also contains important information about the system (channel-mixing coefficients). The "minimum complete parameter set"[68] for photoionization of a p^6-subshell consists of five matrix elements, four differences of eigen-quantum-defects (in the close-coupling scheme) and the ten independent elements of the orthogonal 5×5 matrix $U_{i\alpha}$. Regarding the ionization of subshells with $l>1$ and $J=0$ [for instance, the $(n-1)d^{10}$ shell of Hg and Cd], six dissociation channels are possible, so that the number of parameters that can be determined experimentally is increased further.[76]

The evaluation procedure for D_i and $\mu_i-\mu_j$ was as follows. For the $^2P_{1/2}$ ion the real quantities D_4, D_5, and $\delta_4-\delta_5$ were determined from $\sigma_{1/2}$, $\beta_{1/2}$, and $\xi_{1/2}$. At those wavelengths where no measured values of β and ρ were available, interpolated experimental values that are also supported by theoretical calculations were used.

The measured quantity A is the mean value weighted with the partial cross sections:

$$A = \frac{A_{1/2}+\rho A_{3/2}}{1+\rho} . \tag{12}$$

Using D_4 and D_5 one gets $A_{1/2}$ according to Eq. (11); then, by use of the measured value of A the parameter $A_{3/2}$ can also be determined [Eq. (12)]. Since no experimental values of A exist between 27.8 and 40.8 eV, $A_{3/2}$ was assumed to be in between its limits $-0.5<A_{3/2}<0.5$ for further considerations.

For the $^2P_{3/2}$ ionic channels only four experimental quantities are available for the determination of D_1, D_2, D_3, $\delta_1-\delta_2$, and $\delta_3-\delta_1$. Therefore, the evaluation proceeded with the approximation that the phases of the two d-continuum functions δ_1 and δ_2 are equal, in other words, the influence of the spin-orbit interaction was assumed to be restricted on the ionic fine-structure splitting and on the difference of the matrix elements D_1 and D_2. The assumption $\delta_1-\delta_2=0$ is justified because the main part of the phase-shift difference [Eq. (2)]—the Coulombic part—vanishes according to Eq. (3). In order to determine all five quantities, another experimental parameter

has to be investigated, for instance, the asymmetry parameter α of the spin-polarization transfer A, for which preparations are in progress at BESSY.

The sign convention of the reduced matrix elements has been taken into account when the phase differences $\delta_4-\delta_5$ and $\delta_3-\delta_1$ were determined (D_1, D_2, D_3, D_4 positive, D_5 negative at the ionization threshold). The results are shown in Figs. 1–4 and are explained in the following. The error bars represent uncertainties of all experimental quantities involved in the computation. They are connected smoothly by a tentative curve regardless of autoionization resonances in this spectral range converging to the ns^2 threshold. Note that for Kr the values at $h\nu=26.86$ and 27.77 eV are close to the resonance structures at 26.8 eV (Ref. 77) and 27.6 eV (Ref. 78) and for Ar the value at $h\nu=26.86$ eV lies on the high-energy side of the strong $3s\,3p^6 4p\ ^1P_1$ resonance at 26.62 eV.[50] This may be the reason why some of the error bars at these energies deviate slightly from the tentative curve. These data in the open ionization continuum represented by the solid curve may be compared with results below and slightly above the thresholds (vertical dashed lines) where the data were computed from the D_α, μ_α, and $U_{i\alpha}$—data of several authors according to Eq. (1).

C. Ar $3p^6$ photoionization

The *dotted* curves in Figs. 1 and 2 were calculated from energy independent D_α and $U_{i\alpha}$ and energy-dependent eigen-quantum-defects μ_α. These MQDT quantities are *ab initio* values determined by Fano and Lee[68] in a Hartree-Fock calculation. (In the lower part of Fig. 2, $\mu_4-\mu_5$, the dotted curve is not plotted since it is identical to the dashed-dotted curve.) The *dashed-dotted* curves are based on constant D_α and $U_{i\alpha}$ and the energy dependent μ_α of Lee and Lu.[69] These quantities have been found semiempirically by a fitting procedure resulting from spectroscopic data in the discrete spectral range, from the photoionization cross section in the autoionization region, and from the cross section and branching ratio in the open continuum. The data were calculated at the $^2P_{3/2}$ threshold (left vertical line). A comparison with the results of this work shows that the energy dependence of these two curves with constant D_α and $U_{i\alpha}$ (Refs. 68 and 69) is too weak to allow an extrapolation far beyond the ionization threshold. Especially for D_3 and D_5 and for the differences of the modified eigen-quantum-defects of Ar, the extrapolated straight lines deviate strongly from the measured values. On the other hand, the tentative curves extrapolated to lower energies fit smoothly to the straight lines, especially with regard to the differences of the quantum defects. The *solid* lines that have been worked out by use of a constant $U_{i\alpha}$ matrix (determined at the $^2P_{1/2}$ threshold) and energy dependent D_α and μ_α show good agreement at the ionization threshold. These MQDT quantities were obtained *ab initio* by Johnson *et al.*[22] in RRPA. In order to allow a better comparison with the measured points the curves were drawn smoothly across the autoionization range between the ionization thresholds where, in reality, the D_i and δ_i show a pronounced resonance behavior (see Sec. V) and only the close-coupling parameters D_α and μ_α vary weakly. Similarly the *dashed* curves agree well with the experimental points in the continuum. These curves are based on a parameter set by
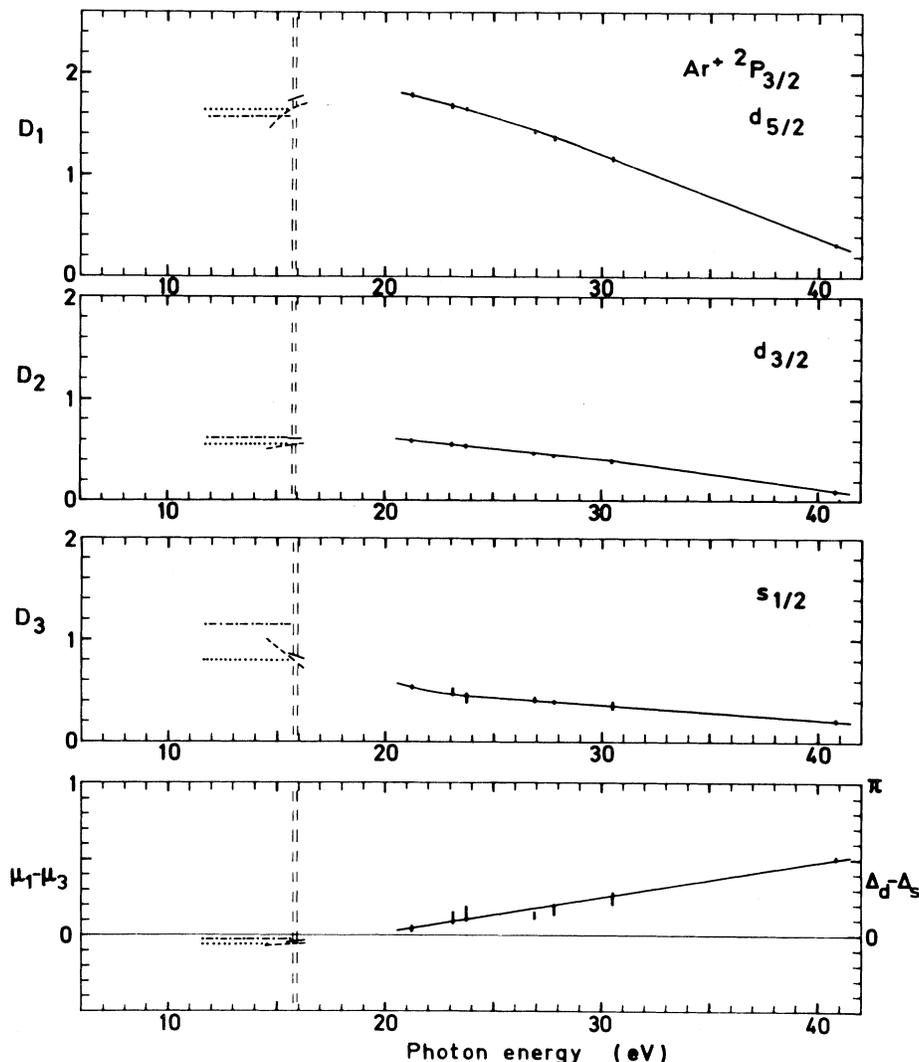
FIG. 1. Modified MQDT quantities D_i and $\mu_i - \mu_j$ (matrix elements and phase-shift differences), corresponding to the Ar^+ $^2P_{3/2}$ ion. Error bars connected by a smooth curve are the result of this work. Vertical dashed lines indicate the ionization thresholds. Curves in the discrete spectral range were calculated from the following parameter sets: $\cdots$, Fano and Lee (Ref. 68); $-\cdot-$, Lee and Lu (Ref. 69); $---$, Lee (Ref. 3); ———, Johnson et al. (Ref. 22).

Lee[3] in which the D_α and μ_α as well as the elements of the transformation matrix $U_{i\alpha}$ depend on the energy (calculated with an extended Hartree-Fock procedure[68]).

D. Kr $4p^6$ photoionization

For Kr (Figs. 3 and 4), as well as for Ar, MQDT parameters D_α and μ_α calculated in RRPA are available.[22] The corresponding modified quantities are the solid curves extrapolated smoothly across the autoionization range. Despite the strong energy dependence of these curves which is due to the strong energy dependence of D_α, especially for $\alpha = 3$ and 5, the connection to the measured points above the second ionization threshold is generally good.

The two dashed-dotted curves originate from semi-empirical data of Geiger,[20,79] obtained experimentally by energy-loss spectra of keV electrons. The weakly energy-dependent straight lines ($-\cdot-$) were determined from a parameter set of constant D_α and $U_{i\alpha}$ and energy dependent μ_α,[79] the more strongly energy-dependent lines ($-\cdot\cdot-$) are based on the same $U_{i\alpha}$ and μ_α, but different dipole amplitudes D_α, of which D_α ($\alpha = 5$) is energy dependent. This curve shows a much better connection to the fitted curve above the threshold, especially for Kr D_3 and D_5. An extrapolation of the matrix elements obtained in the discrete spectral range into the ionization continuum seems to make sense only when the eigen-quantum-defects μ_α as well as the transition amplitudes D_α are chosen to be energy dependent. The differences of the modified eigen-
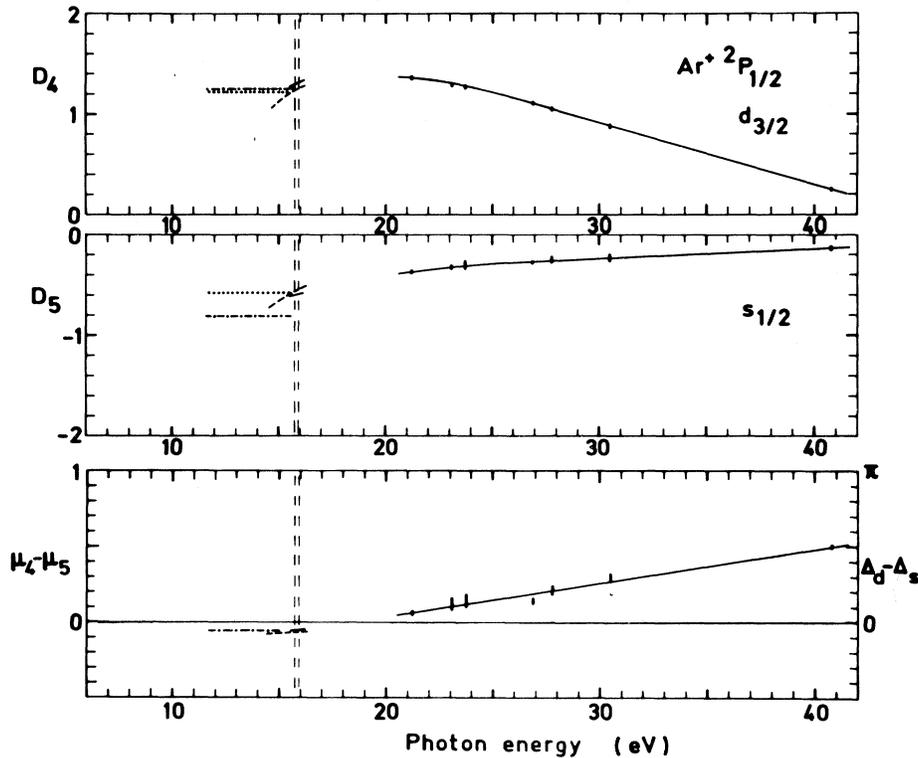
FIG. 2. Modified MQDT quantities D_i and $\mu_i - \mu_j$, same as Fig. 1 but corresponding to the Ar$^+$ $^2P_{1/2}$ ion (see caption of Fig. 1). In the lower part, $\mu_4 - \mu_5$, the dotted and dashed-dotted curves are identical.

quantum-defects $\mu_1 - \mu_3$ and $\mu_4 - \mu_5$ of Kr, however, are identical for both parameter sets of Geiger[20,79] and show excellent agreement with the measured points of this work.

E. Comparison with the Xe 5p^6 photoionization

If one compares the results obtained for Ar and Kr with the MQDT analysis of Xe,[4] one also finds that in no case for Xe does the linear extrapolation of the modified close-coupling data from the discrete part far into the open continuum yield a reasonable good agreement. The energy dependence of the matrix elements D_i above the threshold for Xe is similar to Ar and Kr. The Cooper minimum (change of sign of the matrix element) in D_1, D_2, and D_4 occurs at higher energies for Ar and Kr, while D_2 for Xe already changes sign at 35 eV photon energy. Generally, the MQDT quantities of different authors below the threshold differ much less and their connection to the continuum is much better for Ar than for Kr and Xe. This is due to the fact that for Ar the LS classification for the close-coupling channels is a good approximation. The $U_{i\alpha}$ matrix, therefore, deviates only slightly from the analytically known jj-LS transformation matrix.[80]

One important result that has already been verified for Xe is the fact that the differences of the modified eigen-quantum-defects $\mu_1 - \mu_3$ and $\mu_4 - \mu_5$ in the open continu-

um are identical within the error limits. This means that the difference $\Delta_d - \Delta_s = \pi(\mu_d - \mu_s)$ is independent of whether the photoelectron originated from a $p_{3/2}$ or a $p_{1/2}$ initial subshell. Adding the Coulomb phase shifts [Eq. (2)] that differ because of the different kinetic energies of the photoelectrons from the $p_{1/2}$ and $p_{3/2}$ initial state [Eq. (3)], one obtains the total phase difference $\delta_d - \delta_s$. Interpreting $\delta_d - \delta_s$ as the phase difference of the continuum wave functions seems obvious since the initial electronic state seems to have no marked influence on it.

The excellent agreement between the differences of the modified eigen-quantum-defects $\mu_4 - \mu_5$ obtained above and below the ionization thresholds is demonstrated in Fig. 5 for Ar, Kr, and Xe. The tentative curves on the right-hand side of the thresholds (vertical dashed lines) have one representative error bar only. The curves on the left-hand side of the thresholds are based on the MQDT parameter sets of Lee[3] (Ar) and Geiger[20] (Kr and Xe).

IV. APPLICATION OF THE RESULTS FOR THE PREDICTION OF $A_{1/2}$ AND $A_{3/2}$ AND COMPARISON WITH ab initio CALCULATIONS

This section demonstrates how the results of Sec. III can be applied to predict the behavior of other experimental parameters that, up until now, could not be measured. The parameter A was introduced as being the averaged spin polarization of all photoelectrons extracted regardless
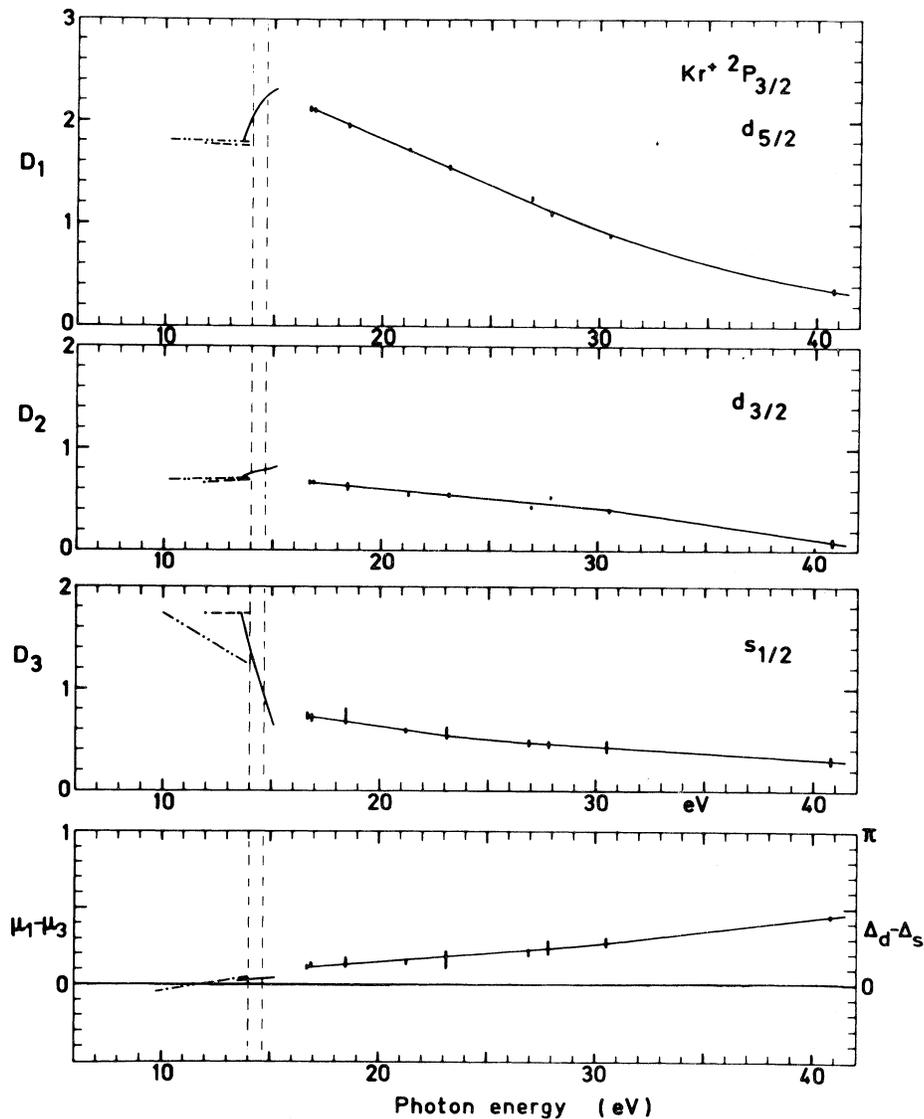
FIG. 3. Modified MQDT quantities D_i and $\mu_i - \mu_j$, same as Fig. 1 but corresponding to the $\mathrm{Kr^+}\,^2P_{3/2}$ ion. Error bars connected by a smooth curve are the result of this work. Parameter sets are as follows: $—\cdot\cdot—$, Geiger (Ref. 20); $—\cdot—$, Geiger (Ref. 79); $———$, Johnson et al. (Ref. 22). $\mu_i - \mu_j$ curves with the parameter sets of Geiger are identical.

of their direction of emission. Due to the experimental arrangement for its measurement (Sec. II) no energy analysis of the photoelectrons could be performed. Therefore, the photoelectrons from the $p_{3/2}$ and $p_{1/2}$ subshells of the rare gases having slightly different energies could not be separated and the measured spin polarization is a net value of both fine-structure components weighted with their partial cross sections [Eq. (12)]. With the use of the results of Sec. III the parameter A can now be determined separately for the two fine-structure components ($A_{3/2}$ and $A_{1/2}$).

The existence of a spin polarization of photoelectrons from unpolarized atoms is a consequence of the spin-orbit interaction. If the fine structure is not resolved the polari-

zation vanishes in the nonrelativistic model.[55,81] Therefore, the sign of the spin polarization of the two sorts of electrons has to be different and their ratio $A_{3/2}/A_{1/2}$ in this approximation must be $1/(-2)$, whereas the branching ratio $\sigma_{3/2}/\sigma_{1/2}$ is the statistical ratio 2/1. [The same considerations are also valid for the spin parameter $\xi_{3/2}$ and $\xi_{1/2}$ (Ref. 53).] Therefore, deviations of the measured spin polarization A from zero indicate deviations from the nonrelativistic theory. In fact, A increases in the sequence Ar, Kr, Xe [Ar—1%; Kr—3% (Ref. 17); Xe up to —15% (Ref. 18)]. Figures 6 and 7 show the results for $A_{1/2}$ and $A_{3/2}$ for the valence shells Ar $3p^6$ and Kr $4p^6$, respectively, as error bars. (The evaluation procedure for $A_{1/2}$ and $A_{3/2}$ from the experimental data is described in Sec. III B.) The
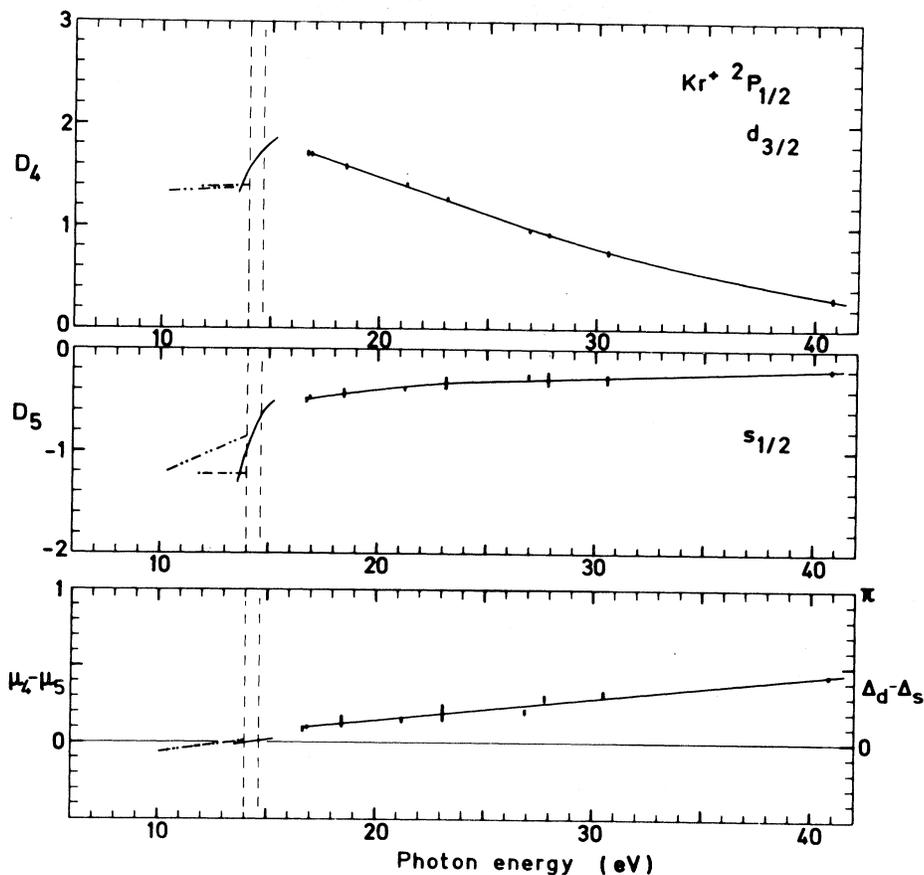
FIG. 4. Modified MQDT quantities D_i and $\mu_i - \mu_j$, same as Fig. 3 but corresponding to the $Kr^+\,{}^2P_{1/2}$ ion.

figures confirm the prediction that the sign is different for the two fine-structure components. A quantitative comparison shows that for Ar the ratio $1/(-2)$ is fulfilled within the error limits for each error bar. These results may be compared with two *ab initio* calculations in nonrelativistic RPAE (Ref. 82) of Cherepkov[2,83] (only $A_{1/2}$) and in the relativistic RRPA of Huang *et al.*[59,60] These theories take into account the influences of many-electron

correlations on the photoionization process (intrashell correlations within the ionized $3p^6$ shell and intershell correlations with the $2p^6$ and $3s^2$ subshells).

The agreement of both curves with the error bars is good. According to Cherepkov[83] the wavelength shift between the two $A_{1/2}$ curves is due to a different position of the Cooper minimum in the ϵd-continuum channel at approximately 25 nm which is very sensitive to correlation
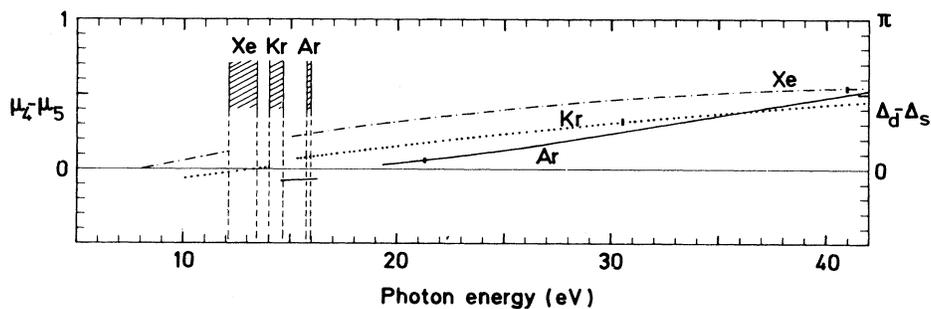
FIG. 5. Comparison of $\mu_4 - \mu_5$ [$(\Delta_d - \Delta_s)/\pi$ for the ${}^2P_{1/2}$ ion] for Ar, Kr, and Xe. Curves below the ionization thresholds have been taken from Lee (Ref. 3) (Ar) and Geiger (Ref. 20) (Kr and Xe). Autoionization regions are hatched.
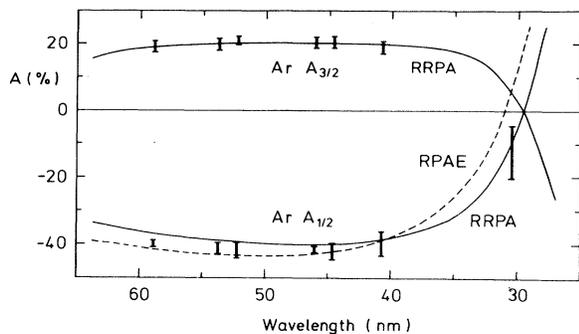
FIG. 6. Spin-polarization transfer A of photoelectrons of Ar $3p^6$ with the residual ion $^2P_{3/2}$ and $^2P_{1/2}$ for $A_{3/2}$ and $A_{1/2}$, respectively. Error bars are this work, determined according to Eqs. (11) and (12); solid curve, RRPA calculation of Huang *et al.* (Refs. 59 and 60); dashed curve, RPAE calculation of Cherepkov (Refs. 2 and 83).

effects. Both theories use experimental thresholds. For Kr (Fig. 7) the ratio $1/(-2)$ is not exactly fulfilled as the spin-orbit interaction also influences the continuum states. For comparison only the RRPA calculation of Huang *et al.*[59,60] is available. In this calculation the many-electron correlations with the $3p^6$, $4s^2$, and $3d^{10}$ subshells are included. To get a quantitative agreement with the error bars it seems that the curves have to be shifted to longer wavelengths. Since experimental thresholds are used, this shift seems to indicate the necessity of including further correlations as these are known to strongly influence the wavelength dependence of the β parameter.[57] The shift is, however, less pronounced in the other dynamical parameters ξ (Refs. 53 and 58) and β (Ref. 57) whose agreement with experiment is satisfactorily good.

One important result is that the highest values of the spin polarization measured or calculated for Ar $3p^6$, Kr $4p^6$, and Xe $5p^6$ (Refs. 4, 55, 59, and 60) are nearly identical. The absolute value of the spin polarization, therefore, is independent of the strength of the spin-orbit interaction, whereas the fine-structure splitting (Ar, 0.18
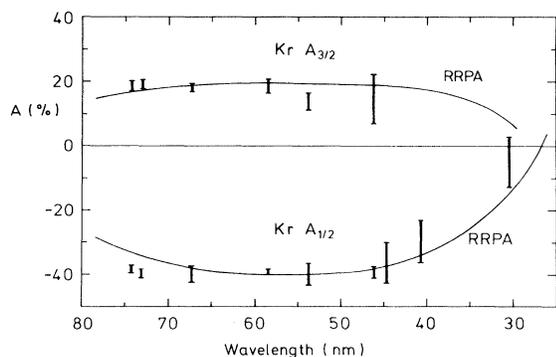
FIG. 7. Same as Fig. 6 for Kr $4p^6$. An RPAE calculation is not available.

eV; Kr, 0.67 eV; Xe, 1.32 eV) depends enormously on it. To get highly spin-polarized photoelectrons one does not need a strong spin-orbit interaction but only a separation of the spin-orbit-induced fine-structure components in the experiment.

V. DISCUSSION OF THE EXPERIMENTAL AND THEORETICAL RESULTS IN THE AUTOIONIZATION REGION OF Ar AND Kr

In the energy region between the first two ionization thresholds of the rare gases belonging to the fine-structure-split ionic configurations $^2P_{3/2}$ and $^2P_{1/2}$, those three continuum channels for photoelectrons from the $p_{3/2}$ subshell are open and those two channels for electrons from the $p_{1/2}$ shell are closed. They may interact, however, with the open channels by autoionization processes, resulting in two series of Beutler-Fano resonances converging to the $^2P_{1/2}$ threshold. This pronounced resonance structure can be seen not only in the cross section but also in other quantities measured so far [β parameter for Xe (Ref. 16); spin polarization A for Ar, Kr (Ref. 17), and Xe (Ref. 18)].

In this section the experimental results of the spin polarization A will be compared with MQDT calculations and for Kr an analysis of the first three resonances of both series will be presented, which cannot be "complete" in the way developed in Sec. III because on the basis of the two parameters σ and A that have been measured so far the evaluation of three matrix elements and two phase-shift differences is, of course, not possible.

For the autoionization spectrum the connection between the close-coupling matrix elements D_α and eigen-quantum-defects μ_α (that vary only smoothly in this region) and the corresponding modified loose-coupling parameters D_i and μ_i is more complicated than for the continuous spectrum (cf. Sec. III). Three "collisional eigen-channels" ρ ($\rho = 1, 2, 3$) are introduced in which all interaction between the five close-coupling channels α takes place. The system transformation between the eigenchannels and the loose-coupling dipole amplitudes D_i is performed by the following equation:

$$D_i e^{i\pi\mu_i} = \sum_{\rho=1}^{3} T_{i\rho} e^{i\pi\tau_\rho} D_\rho \, , \tag{13}$$

where i takes the values 1,2,3 for the $p_{3/2}$ subshell, $\pi\tau_\rho$ are the short-range eigenphases of the three open eigenchannels ρ, D_ρ denote the corresponding eigenamplitudes, and $T_{i\rho}$ is the orthogonal transformation matrix between the eigenchannels ρ and the open continuum channels i. All three quantities τ_ρ, D_ρ, and $T_{i\rho}$ ($\rho = 1, 2, 3$) may be obtained from the close-coupling parameters μ_α, D_α, and $U_{i\alpha}$ ($\alpha = 1, \ldots, 5$), according to Lee *et al.*,[70,84] Geiger,[19,20] and Dill.[21]

A. Kr $4p^6$ photoionization

Figure 8 (lower part) shows the results of the spin-polarization measurements at Kr as vertical error bars. The bandwidth of the radiation is indicated as a horizontal error bar at some points only. For comparison, in the upper part the relative cross section of Saile[14] (solid curve) fitted to an absolute value[13] in the maximum of the first d
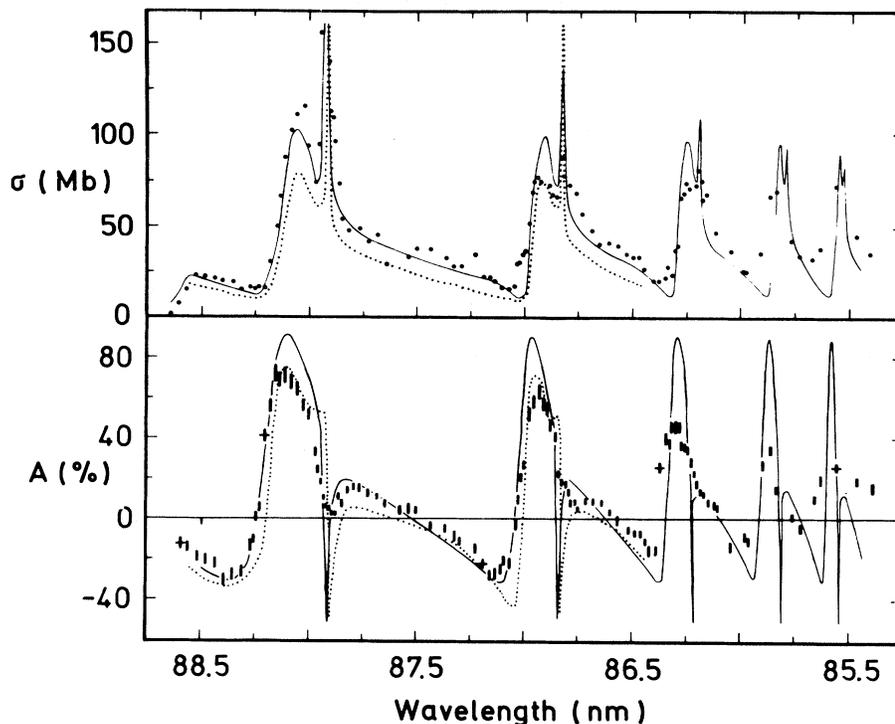
FIG. 8. Kr $4p^6$ photoionization in the autoionization region. Upper half: cross section σ. Solid curve, measurements of Refs. 13 and 14; points, this work and Ref. 17. Lower half: spin-polarization transfer A. Solid curve, RRPA calculation of Johnson et al. (Ref. 22); error bars, this work and Ref. 17. Dotted curves: this work, based on MQDT parameters of Geiger (Ref. 20).

resonance is plotted. The points indicate the electron intensity obtained during the polarization measurements. Similar to the cross section the electron spin polarization shows a pronounced resonance structure with changes of sign from -30% to $+75\%$ in a wavelength region smaller than 0.1 nm. The structure is periodical and gets smaller with shorter wavelengths due to insufficient resolution.

The solid curve in the lower part is based on an MQDT calculation of Johnson et al.[22] with parameters obtained ab initio in RRPA. In this calculation correlations within the $4p^6$ and with the $4s^2$ and $3d^{10}$ subshells are included. Aside from the different heights of the positive and negative polarization maxima in the d and s resonances (the discrepancies in the sharp s resonances are due to an insufficient experimental resolution) the curve is in excellent agreement with the experimental results, especially concerning the position of the resonances and of the change of sign of the polarization, both of which are very sensitive to correlation effects. The theory employs experimental thresholds. The dotted curves in the upper and lower halves of Fig. 8 represent MQDT calculations based on the semiempirical parameters of Geiger[20] obtained from experimental line positions and oscillator strengths in the discrete spectrum [energy-independent matrix elements D_α ($\alpha = 1, \ldots, 4$) and $U_{i\alpha}$ energy-dependent eigen-quantum-defects μ_α and D_α ($\alpha = 5$); the same parameter set that led to the dashed-double-dotted lines in Figs. 3 and 4]. Although the general agreement with the experimental

values is good there remains a small shift of the curves to shorter wavelengths, a fact that was already observed for Xe also.

A complete description of the photoionization process in the autoionization region by determination of the three modified matrix elements D_i ($i = 1,2,3$) and the two phase-shift differences $\delta_1 - \delta_2$ and $\delta_3 - \delta_1$ is not possible at present since this would require the knowledge of three other experimental quantities besides σ and A. A combination of these two quantities yields, however, further conclusions on the dynamics of the photoionization process. For this, the five quantities mentioned above are replaced by the three complex matrix elements S_1, S_2, and S_3. In the formalism of the angular-momentum transfer developed by Fano and Dill[21,85,86] which has recently been extended to the treatment of spin polarization,[61] these matrix elements determine the parity-favored transitions [angular-momentum transfer $t = 1$ from the photon to the electron with angular momentum $l = 0$ (S_3) and $l = 2$ (S_1), respectively] and the parity-unfavored transition S_2 ($t = 2, l = 2$). The reason for the introduction of these quantities is that combinations of them are simple functions of the experimental quantities σ and A (Ref. 4). The cross section is proportional to $\sum_{i=1}^{3} |S_i|^2$. The quantity plotted in Fig. 9, $4/3\sigma(A + \frac{1}{2})$, is proportional to $|S_1 + S_2|^2$; thus this quantity is influenced by interferences between S_1 and S_2. The solid curve in Fig. 9 is based on experimental results for σ and A with representa-
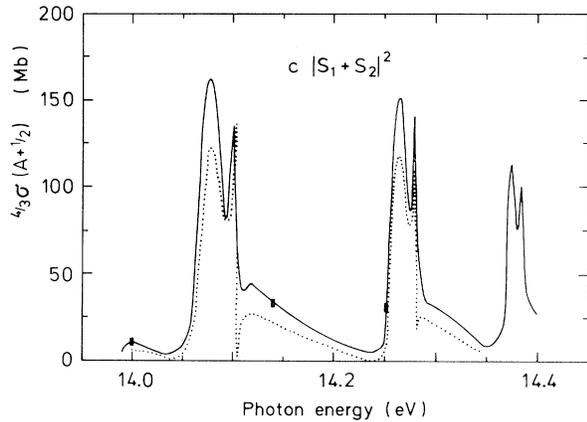
FIG. 9. $Kr\,4p^6$ photoionization in the autoionization region. Quantity $c\,|S_1+S_2|^2$ determined from experimental results of σ and A (full curve) and from MQDT results (Ref. 20) (dotted curve).

tive error bars shown at some points only, while the dotted curve was computed from the dotted curves in Fig. 8. Both experimental and theoretical curves show constructive and destructive (in the dotted curve down to zero) interferences of S_1 and S_2. The agreement of the shape of the two curves is good, while the differences in the absolute height are due to the differences in the cross-section scales of Geiger and Saile[14] (Fig. 8). As mentioned above, S_1 and S_2 denote the parity-favored and parity-unfavored transitions into the d continua ($l=2$), therefore, the results in Fig. 9 are determined only by ϵd-matrix elements. In spite of this, the series of the sharp resonances, identified earlier as s resonances, can clearly be seen. This is strong evidence for a pronounced channel mixing between the autoionizing ns channel and the ϵd-continuum channels (quadrupole coupling[69]).

B. Ar $3p^6$ photoionization

Figure 10(b) shows the results of the measurements obtained in the autoionization region of $Ar\,3p^6$ as points (upper part) and error bars (lower part). The resonance structure is much less pronounced than for Kr, due to insufficient resolution. (The bandwidth is indicated as a horizontal error bar.) The results of theoretical calculations and of a high-resolution cross-section measurement are plotted in Fig. 10(a). The dashed curves represent the theoretical prediction by Lee,[3] the dashed-dotted curve indicates the cross section measured by Hudson and Carter[7] with a bandwidth of 0.004 nm indicated as horizontal error bar, and the full curve shows the RRPA calculation of the spin polarization of Johnson et al.[22] Here correlations with the $3p^6$ and $3s^2$ subshell are included. It is interesting to note that the periodic structure of the RRPA curve repeats itself in identical form along the Rydberg series, while the resonance structure in Lee's calculation flattens. This is probably due to a larger energy dependence of the MQDT parameters used by Lee.

The comparison between the theoretical results shown in Fig. 10(a) and the experimental results of this work
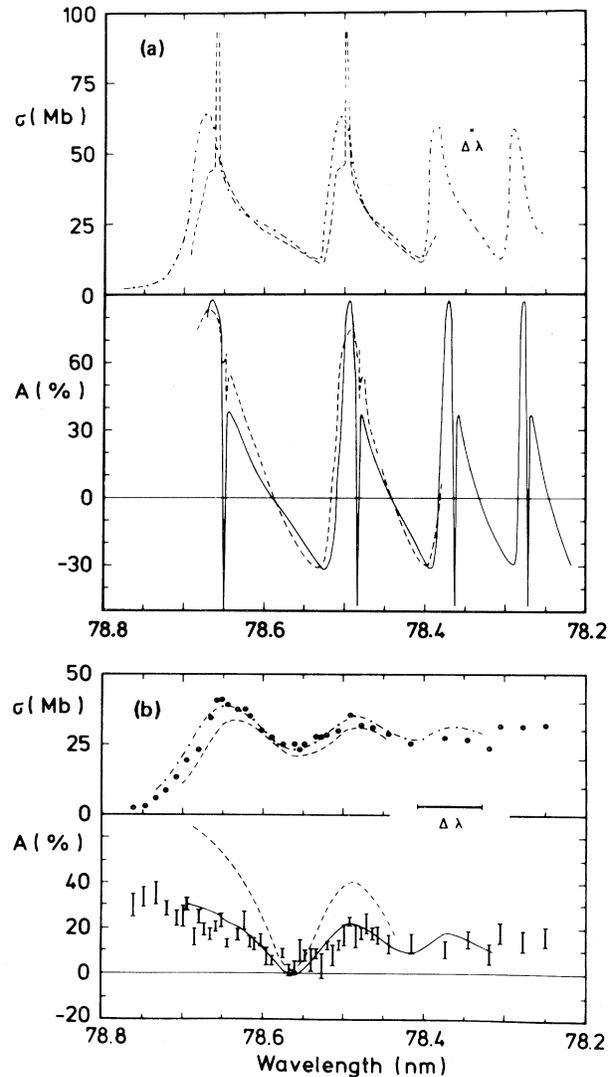
FIG. 10. $Ar\,3p^6$ photoionization in the autoionization region. (a) Upper half: cross section σ. Dashed-dotted curve, measurement of Hudson and Carter (Ref. 7); dashed curve, MQDT calculaton of Lee (Ref. 3). Lower half: spin-polarization transfer A. Solid curve, RRPA calculation of Johnson et al. (Ref. 22); dashed curve, MQDT calculation of Lee (Ref. 3). (b) Same as (a) but the curves are convoluted with a triangular profile of 0.08 nm FWHM (experimental resolution). Points (upper half) and error bars (lower half) are the experimental results of this work and Ref. 17, respectively.

[Fig. 10(b)] has to be performed on the basis of the experimental resolution. Therefore, the curves of Fig. 10(a) have been convoluted with a triangular profile of 0.08 nm full width at half maximum (FWHM). The result is plotted in Fig. 10(b) together with the experimental results. While the cross section now shows good agreement with the shape of the electron intensity measurements (points), the convolution procedure of the polarization curves reveals

drastic differences between the calculations: The RRPA calculation (full curve) is in good agreement with the experiment in between the error limits, but the resonance pattern in Lee's prediction (dotted curve) is still too pronounced. The differences between the two convoluted curves, which could not be seen so clearly in Fig. 10(a), are due to the fact that, compared to Lee, the results of Johnson et al. show the following:

(i) smaller resonances in the polarization curve and

(ii) a much more pronounced oscillation in the s resonances, down to values of -50%.

Combined with a high cross section in the s resonance which serves as a weighting factor in the convolution procedure, this is responsible for the fact that in the RRPA curve the resonances become more flattened than in Lee's curve. These differences between the two curves cannot be seen in the corresponding cross-section calculations, which yield practically identical results. Therefore, the same numerical cross-section values (those of Lee) were used for the convolution procedure of both polarization curves. It is interesting to note that Heckenkamp et al.[87] have recently reported a combination of spin-polarization measurement with threshold photoelectron spectroscopy by which the spin polarization of the photoelectrons at the $^2P_{3/2}$ threshold of Ar could be measured with an electron energy bandwidth of 3 meV (0.015 nm). Their result ($A = 38\%$) also shows good agreement with the RRPA calculation, which is further evidence for the validity of this theory.

VI. CONCLUSIONS

In this paper the importance of experimental photoelectron spin-polarization data was demonstrated so as to complement the cross-section data in order to form a complete parameter set for the photoionization from which such basic quantities as transition matrix elements and phase-shift differences of continuum wave functions can be extracted. The results obtained for Ar$3p^6$ and Kr$4p^6$ photoionization over a wide energy range could be compared with oscillator strengths and eigen-quantum-defects in the discrete spectral range. The connection across the ionization threshold was established by means of the MQDT which describes the photoabsorption and photoionization process by a small set of parameters: dipole amplitudes D_α, eigen-quantum-defects μ_α, and a tran-

sition matrix $U_{i\alpha}$. The best overall agreement with the experimental data is achieved if these parameters are chosen to be energy dependent. The results of this paper show that the D_α and μ_α (or the corresponding modified quantities D_i and μ_i) may be extrapolated across the ionization threshold and may be used to reproduce even such complex structures as autoionization resonances where five interacting channels have to be taken into account. This is a striking test for the validity of the MQDT approach. The employment of the correlated and relativistic RPA to work out the (ab initio) MQDT parameters yields best agreement with experimental results both in the autoionization region and in the open continuum. Correlation effects in the form of a strong quadrupole coupling between the s and d channels could be seen clearly affecting the autoionizing processes for Kr. Relativistic effects, on the other hand, show increasing importance in the sequence of Ar, Kr, Xe.

Up until now, only two spin-polarization parameters, A and ξ, could be measured due to intensity reasons. Whereas the analysis of the $p_{1/2}$-subshell photoionization is complete, the evaluation of the five parameters governing the $p_{3/2}$-subshell photoionization process out of four experimental quantities could only be performed in a small approximation about the influence of the spin-orbit interaction onto the continuum states. This assumption is not necessary in cases where less than five parameters have to be determined, as was demonstrated in this paper at the $p_{1/2}$ subshell or at the Hg $6s^2$ valence shell as recently reported.[64,88] Experimental work is in progress at the German dedicated source of synchrotron radiation BESSY for the measurement of all three components of the spin polarization vector in angle-resolved photoelectron spectroscopy with the use of circularly polarized light. These measurements will enable us to complete this analysis and to extend it to other atomic and molecular systems.

[1]K. N. Huang, Phys. Rev. A **22**, 223 (1980).

[2]N. A. Cherepkov, Zh. Eksp. Teor. Fiz. **65**, 933 1973 [Sov. Phys.—JETP **38**, 463 (1974)].

[3]C. M. Lee, Phys. Rev. A **10**, 1598 (1974).

[4]U. Heinzmann, J. Phys. B **13**, 4353 (1980); **13**, 4367 (1980).

[5]H. Beutler, Z. Phys. **93**, 177 (1935).

[6]R. E. Huffman, Y. Tanaka, and J. C. Larrabee, J. Chem Phys. **39**, 902 (1963).

[7]R. D. Hudson and V. L. Carter, J. Opt. Soc. Am. **58**, 227 (1968).

[8]K. Yoshino, J. Opt. Soc. Am. **60**, 1220 (1970).

[9]P. H. Metzger and G. R. Cook, J. Opt. Soc. Am. **55**, 516 (1965).

[10]K. Radler and J. Berkowitz, J. Chem. Phys. **70**, 216 (1979); **70**, 221 (1979).

[11]J. Berkowitz, *Photoabsorption, Photoionization and Photoelectron Spectroscopy* (Academic, New York, 1979).

[12]R. E. Huffman, Y. Tanaka, and J. C. Larrabee, Appl. Opt. **15**, 947 (1963).

[13]V. L. Carter and R. D. Hudson, J. Opt. Soc. Am. **63**, 733

(1973).

[14]V. Saile, Ph.D. thesis, Universität München, 1976 (unpublished).

[15]K. Yoshino and Y. Tanaka, J. Opt. Soc. Am. 69, 159 (1979).

[16]J. A. R. Samson and J. L. Garnder, Phys. Rev. Lett. 31, 1327 (1973).

[17]U. Heinzmann and F. Schäfers, J. Phys. B 13, L415 (1980).

[18]U. Heinzmann, F. Schäfers, K. Thimm, A. Wolcke, and J. Kessler, J. Phys. B 12, L679 (1979).

[19]J. Geiger, Z. Phys. A 276, 219 (1976).

[20]J. Geiger, Z. Phys. A 282, 129 (1977).

[21]D. Dill. Phys. Rev. A 7, 1976 (1973).

[22]W. R. Johnson, K. T. Cheng, K. N. Huang, and M. Le Dourneuf, Phys. Rev. A 22, 989 (1980).

[23]R. E. Huffman, Y. Tanaka, and J. C. Larrabee, Appl. Opt. 2, 947 (1963).

[24]O. P. Rustgi, E. J. Fisher, and C. H. Fuller, J. Opt. Soc. Am. 54, 745 (1964).

[25]J. A. R. Samson, Adv. At. Mol. Phys. 2, 178 (1966).

[26]R. D. Hudson and L. J. Kieffer, At. Data 2, 205 (1970).

[27]G. V. Marr and J. B. West, At. Data Nucl. Data Tables 18, 497 (1976).

[28]F. J. Comes and H. G. Sälzer, Z. Naturforsch. 119, 1230 (1964).

[29]J. A. R. Samson and R. B. Cairns, Phys. Rev. 173, 80 (1968).

[30]J. A. R. Samson, J. L. Gardner, and A. F. Starace, Phys. Rev. A 12, 1459 (1975).

[31]J. Berkowitz, H. Ehrhardt, and T. Tekaat, Z. Phys. 200, 69 (1967).

[32]D. A. Vroom, A. R. Comeaux, and J. W. McGowan, Chem. Phys. Lett. 3, 467 (1969).

[33]J. W. McGowan, D. A. Vroom, and A. R. Comeaux, J. Chem. Phys. 51, 5626 (1969).

[34]J. A. R. Samson, Philos. Trans. R. Soc. London, Sect. A 268, 141 (1970).

[35]R. Morgenstern, A. Niehaus, and M. W. Ruf, Chem. Phys. Lett. 4, 635 (1970).

[36]T. A. Carlson and A. E. Jones, J. Chem. Phys. 55, 4913 (1971).

[37]H. Hotop and A. Niehaus, Chem. Phys. Lett. 8, 497 (1971).

[38]A. Niehaus and M. W. Ruf, Z. Phys. 252, 84 (1972).

[39]R. T. Poole, J. Liesegang, J. G. Jenkin, and R. C. G. Leckey, Vacuum 22, 499 (1972).

[40]J. L. Dehmer, W. A. Chupka, J. Berkowitz, and W. T. Jivery, Phys. Rev. A 12, 1966 (1975).

[41]D. C. Mason, D. M. Mintz, and A. Kuppermann, Rev. Sci. Instrum. 48, 926 (1977).

[42]F. J. Leng and G. L. Nyberg, J. Phys. E 10, 686 (1977).

[43]J. Kreile and A. Schweig, J. Electron Spectrosc. Relat. Phenom. 20, 191 (1980).

[44]P. Mitchell and K. Codling, Phys. Lett. 38A, 31 (1972).

[45]M. J. Lynch, K. Codling, and A. B. Gardner, Phys. Lett. 43A, 213 (1973).

[46]W. S. Watson and D. T. Stewart, J. Phys. B 7, L466 (1974).

[47]R. G. Houlgate, J. B. West, K. Codling, and G. V. Marr, J. Electron Spectrosc. Relat. Phenom. 9, 205 (1976).

[48]D. L. Miller, J. D. Dow, R. G. Houlgate, G. V. Marr, and J. B. West, J. Phys. B 10, 3205 (1977).

[49]K. Codling, J. B. West, A. C. Parr, J. L. Dehmer, and R. L. Stockbauer, J. Phys. B 13, L693 (1980).

[50]M. O. Krause, T. A. Carlson, and P. R. Woodruff, Phys. Rev. A 24, 1374 (1981).

[51]D. M. P. Holland, A. C. Parr, D. L. Ederer, J. L. Dehmer, and J. B. West, Nucl. Instrum. Methods 195, 331 (1982).

[52]D. L. Ederer, A. C. Parr, J. B. West, D. Holland, and J. L. Dehmer, Phys. Rev. A 25, 2006 (1982).

[53]U. Heinzmann, G. Schönhense, and J. Kessler, Phys. Rev. Lett. 42, 1603 (1979); J. Phys. B 13, L153 (1980).

[54]N. A. Cherepkov, J. Phys. B 11, 3117 (1978).

[55]N. A. Cherepkov, J. Phys. B 12, 1279 (1979).

[56]N. A. Cherepkov, J. Phys. B 13, L181 (1980).

[57]W. R. Johnson and K. T. Cheng, Phys. Rev. A 20, 978 (1979).

[58]K. N. Huang, W. R. Johnson, and K. T. Cheng, Phys. Rev. Lett. 43, 1658 (1979).

[59]K. N. Huang, W. R. Johnson, and K. T. Cheng, Phys. Lett. 77A, 234 (1980).

[60]K. N. Huang, W. R. Johnson, and K. T. Cheng, At. Data Nucl. Data Tables 26, 33 (1981).

[61]H. Klar, J. Phys. B 13, 3117 (1980).

[62]G. Schönhense, F. Schäfers, U. Heinzmann, and J. Kessler, Z. Phys. A 304, 31 (1982).

[63]U. Heinzmann, B. Osterheld, and F. Schäfers, Nucl. Instrum. Methods 195, 395 (1982).

[64]F. Schäfers, G. Schönhense, and U. Heinzmann, Z. Phys. A 304, 41 (1982).

[65]K. T. Lu and U. Fano, Phys. Rev. A 2, 81 (1970).

[66]U. Fano, Phys. Rev. A 2, 353 (1970).

[67]K. T. Lu, Phys. Rev. A 4, 579 (1971).

[68]U. Fano and C. M. Lee, Phys. Rev. Lett. 31, 1573 (1973).

[69]C. M. Lee and K. T. Lu, Phys. Rev. A 8, 1241 (1973).

[70]C. M. Lee, Phys. Rev. A 10, 584 (1974).

[71]U. Fano, J. Opt. Soc. Am. 65, 979 (1975).

[72]A. Sommerfeld, Atombau und Spektrallinien (Vieweg, Braunschweig, 1939).

[73]M. J. Seaton, Proc. R. Soc. London 88, 801 (1966).

[74]M. J. Seaton, J. Phys. B 2, 5 (1969).

[75]S. T. Manson, Adv. Electron. Electron Phys. 41, 43 (1976); 44, 1 (1977).

[76]G. Schönhense, Ph.D. thesis, Universität Münster, 1981 (unpublished).

[77]K. Codling and R. P. Madden, Phys. Rev. A 4, 2261 (1971).

[78]J. A. R. Samson, Phys. Rev. 132, 2122 (1963).

[79]J. Geiger (private communication).

[80]U. Fano and G. Racah, Irreducible Tensorial Sets (Academic, New York, 1959).

[81]N. A. Cherepkov, J. Phys. B 11, L435 (1978).

[82]M. Ya. Amusia and N. A. Cherepkov, Case Stud. At. Phys. 5, 47 (1975).

[83]N. A. Cherepkov, J. Phys. B 13, L689 (1980).

[84]C. M. Lee and W. R. Johnson, Phys. Rev. A 22, 979 (1980).

[85]D. Dill and U. Fano, Phys. Rev. Lett. 29, 1203 (1972).

[86]U. Fano and D. Dill, Phys. Rev. A 6, 185 (1972).

[87]Ch. Heckenkamp, F. Schäfers, U. Heinzmann, R. Frey, and E. W. Schlag, Nucl. Instrum. Methods 208, 805 (1983).

[88]G. Schönhense, U. Heinzmann, J. Kessler, and N. A. Cherepkov, Phys. Rev. Lett. 48, 603 (1982).